



# Colorimetric determination of acidity constant using a paper-based microfluidic analytical device

Maryam Taghizadeh-Behbahani<sup>1</sup> · Bahram Hemmateenejad<sup>1</sup> · Mojtaba Shamsipur<sup>2</sup>

Received: 22 July 2017 / Accepted: 30 November 2017 / Published online: 12 December 2017  
© Institute of Chemistry, Slovak Academy of Sciences 2017

## Abstract

Acid dissociation constant is an important chemical characteristic of organic and inorganic compounds and it affects both chemical properties and biological activities of the molecules. Herein, a very simple, fast and cost-effective method based on microfluidic technology has been reported for colorimetric determination of acidity constants. The designed device works based on pH-metric titration of colorful indicators followed by colorimetric measurements by a smart phone mobile device or a flatbed scanner. So, it does not need sophisticated instrumentation and is accomplished in a very short time (about 1 min). All titration steps are transferred on a star-like designed  $\mu$ PAD device: (1) spotting 0.3  $\mu$ L buffers of different pHs at the end of the channels (reaction zones), (2) spotting a 30  $\mu$ L portion of the indicator on the center of  $\mu$ PAD followed by movement of indicator solution toward the reaction zone by capillary action of the paper. The measured color change of the indicators at the reaction zone is fitted to the Henderson–Hasselbalch equation, through which acidity constants are calculated. The performance of the device was evaluated by measuring acidity constant of 4 indicators including bromothymol blue, bromocresol green, bromocresol purple and phenolphthalein. A very close agreement was achieved between those measured by the suggested device here and the previously reported values. The reproducibility of this method was lower than 5% for relative standard deviation of three replicate measurements.

**Keywords** Microfluidic device · Paper ·  $\mu$ PAD · Acidity constant · Colorimetric

## Introduction

Dissociation constants (i.e., pK<sub>a</sub> values) can be considered as a key factor for realization and quantification of such chemical phenomena as biological activity, biological transport, reaction rates, biological uptake and environmental fate (Čadková et al. 2013; Demiralay et al. 2012; Gluck et al. 1996). Various spectroscopic (Nan et al. 2014), chromatographic (Demiralay et al. 2012), electrophoresis (Gluck, Steele, and Benkö 1996) and potentiometric (Čadková et al. 2013) techniques are available for the determination of acidity constants. However, such traditional methods for

determination of pK<sub>a</sub> are usually expensive and time-consuming, requiring special instruments and needing lots of reagents.

In recent years, the microfluidic technology has been conducted for various purposes, including chemical synthesis, analysis, separation, and diagnosis (Oosterbroek and Van den Berg 2003; Xu et al. 2009). In contrast to the first-generation of microfluidic devices, paper-based microfluidic analytical devices ( $\mu$ PADs), have drawn much attention in recent years were first introduced by Whitesides and co-workers (Martinez et al. 2007). To date,  $\mu$ PADs have been used for different applications including but not limited to food safety assessment (Jokerst et al. 2012), biomarkers of pathogens test (Dungchai et al. 2010; Schilling et al. 2012) and environmental monitoring (Jayawardane et al. 2014; Rattanarat et al. 2014). In  $\mu$ PAD technology, filter paper is utilized as a framework substrate for construction of microstructures and developing unique microfluidic functions. The paper can be simply assembled with different detection methods like colorimetric (Mentele et al. 2012; Gao et al. 2014), chemiluminescence (Yu et al. 2011a; Yu et al. 2011b; Wang et al.

**Electronic supplementary material** The online version of this article (<https://doi.org/10.1007/s11696-017-0357-7>) contains supplementary material, which is available to authorized users.

✉ Bahram Hemmateenejad  
hemmatb@shirazu.ac.ir

<sup>1</sup> Department of Chemistry, Shiraz University, Shiraz, Iran

<sup>2</sup> Department of Chemistry, Razi University, Kermanshah, Iran

2012) and electrochemical methods (Rattanarat et al. 2014; Nie et al. 2010).

In this work, we have tried to improve the classical approach of colorimetric determination of pK<sub>a</sub> using a portable and low-cost  $\mu$ PAD. In this regard, a  $\mu$ PAD based on wax dipping fabrication method (Songjaroen et al. 2011, 2012) was developed for simple and fast determination of the acidity constant of pH indicators. Currently there are different methods for fabrication of  $\mu$ PADs (Li et al. 2010; Xia et al. 2016; Songjaroen et al. 2011) For acidity-base titration, Karita and Takashi (Karita and Kaneta 2014) used a wax printing method since wax is more resistant to acid and base solutions. Wax dipping can be used as an alternative to wax printing when the wax printer machine is not available. The fabricated  $\mu$ PAD needs very low amounts of reagent solutions (indicator and buffer) and the method is quite fast to ensure that each assay needs only about 1 min. Integration of the  $\mu$ PAD with a mobile phone or a webcam can be easily used for quantitative determination of acidity constant with an acceptable accuracy. The designed microfluidic paper-based analytical device ( $\mu$ PAD) operates based on pH-metric titration of colorful indicators that required neither time nor instrumentation. The titration was accomplished within just 1 min. The  $\mu$ PAD has benefits in disposability and portability because it is light, small and inexpensive.

## Experimental

### Chemicals

All reagents were of analytical grade. Sodium hydroxide, acetic acid, phosphoric acid and sodium hydroxide solution were obtained from Merck. Bromothymol blue was purchased from Panreac Química S.A. Merck supplied phenolphthalein. Bromocresol green and boric acid were purchased from Fluka. Bromocresol purple was obtained from Hopkin & Williams Ltd. Filter paper (460 × 570 mm, Chromatography Paper 1CHR, Whatman TM, GE Healthcare Lifesciences, United Kingdom) was used. Deionized water was used for preparation of solutions. Paraffin was purchased from B.D.H. laboratory chemicals division.

Iron mold was fabricated by Alghadir wire cut company (Tehran, Iran). Solutions of  $5.0 \times 10^{-4}$  M of bromothymol blue, bromocresol green and bromocresol purple were prepared by dissolving appropriate weighted mass of the indicators in 1.0 mL of ethanol and then diluting to 10.0 mL with deionized water. 0.01 M solution of phenolphthalein in ethanol was prepared by transferring the appropriate weighted mass of the indicator to a 10-mL volumetric flask and diluting to the mark with ethanol. In order to prepare a universal buffer, a solution of 0.04 M H<sub>3</sub>BO<sub>3</sub>, 0.04 M H<sub>3</sub>PO<sub>4</sub>

and 0.04 M CH<sub>3</sub>COOH was titrated with 0.20 M NaOH to reach to the desired pH.

### Washing the papers

In order to remove contaminations on surface or inside the paper (primarily provided in A4 size), it is washed before fabrication of  $\mu$ PADs. The washing is similar to thin-layer chromatography development; paper is hung in a thin-layer chromatography tank containing distilled water. By moving up the water along the paper, the contaminations are washed and are accumulated at the top edge of the paper. It should be noted that to prevent dust entering and water evaporating, the tank is covered with a plastic bag. After about 12 h development, the top edge containing contaminations are cut and the paper is allowed to dry. After 24 h, the paper is ready to be fabricated.

### Design and fabrication of the $\mu$ PAD

The  $\mu$ PAD pattern was designed via AutoCAD 2015 in a star-like pattern of 9 zones (Fig. S1, ESI<sup>†</sup>). Then, the wax dipping method was applied for creation of hydrophobic barriers in the  $\mu$ PAD (P. Wang et al. 2013). In order to construct a mold for wax dipping, an iron plate was cut into the required pattern and size. In wax dipping procedure, briefly, filter paper was cut into a 2.5 cm × 2.5 cm square piece and placed onto a glass slide. The corresponding iron mold was then put onto the paper and attached using a magnet on the backside of the glass slide. Finally, the assembly was dipped into the melted paraffin. When the paraffin was cooled, the glass slide and iron mold were separated from paper (Fig. S2, ESI<sup>†</sup>) (Songjaroen et al. 2011, 2012). Nine reaction zones and nine corresponding distribution channels with the same diameter and length were constructed (Fig. S2, ESI<sup>†</sup>).

### Acidity constant determination

Each reservoir of the  $\mu$ PAD was first filled with a 0.3  $\mu$ l portion of buffer solution of desired pH. After drying, a 30  $\mu$ l portion of the indicator solution was spotted onto the center of  $\mu$ PAD zone and was allowed to reach to the reaction zone by capillary forces at room temperature (20–25 °C). After about 1.0 min, the color changes at reaction zones were captured using a digital camera. In practical experience, the color of phenolphthalein disappears gradually in an alkaline solution (Fig. 1, ESI<sup>†</sup>). So, the pK<sub>a</sub> value may be varied, depending on the time of measuring the color intensity. Since the appeared color intensity fades over the time, and to have higher sensitivity and reproducibility, the image of  $\mu$ PAD was captured as soon as dye solution reached the reaction zone and filled it (30 s after sample loading).

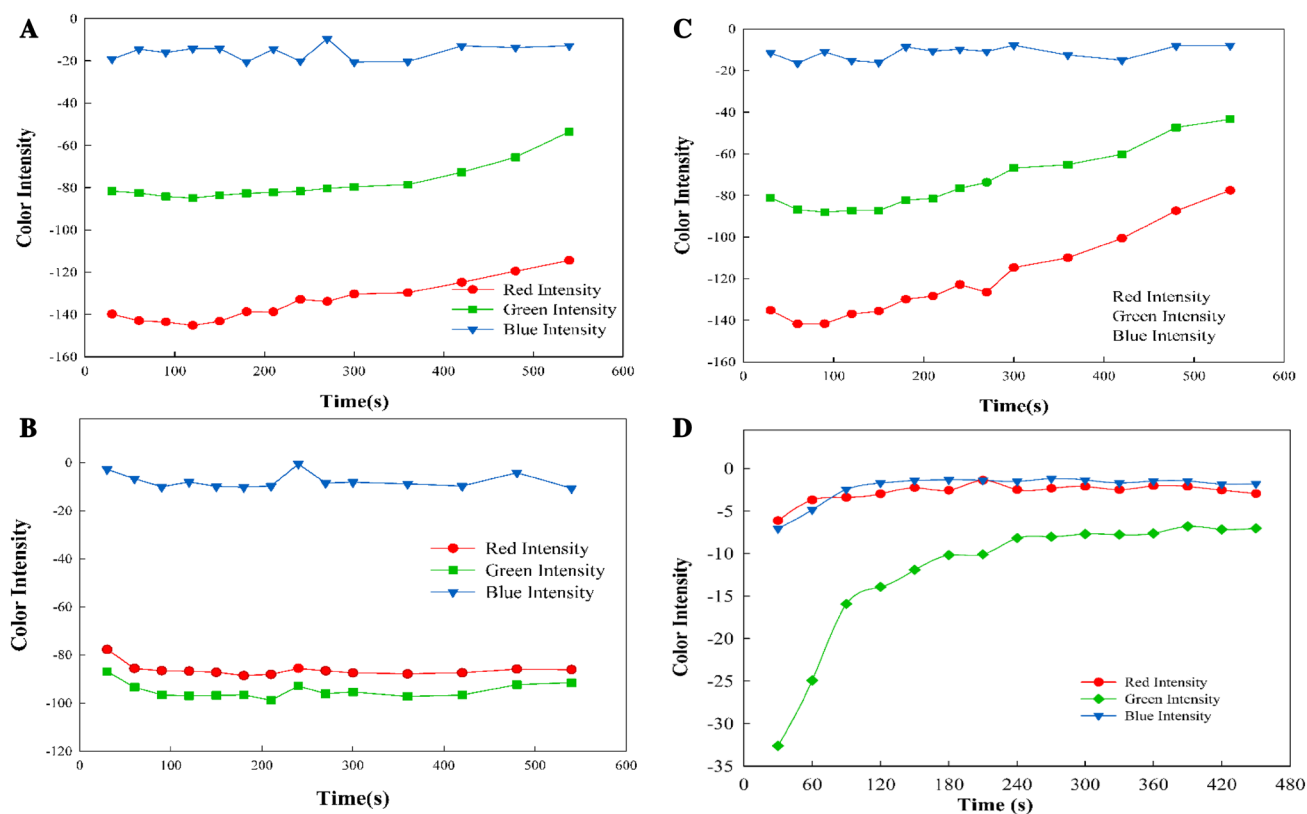


**Fig. 1** The relationship between color intensity and time: **a** BG, **b** BP, **c** BB and **d** PP

Capturing the high-quality reproducible images is a critical step that could affect the precision and the accuracy of acidity constant determination. A home-made imaging cabinet that was previously produced and optimized in our laboratory was used (Hemmateenejad, Farzam, and Mobaraki 2014; Hemmateenejad et al. 2012, 2010). The imaging system is composed of a wooden dark cabinet equipped with a Canon IXUS 145 digital camera (capturing 16-megapixel images) and two white fluorescent tubes. The camera is fixed on the upper and middle of the box, between two fluorescent tubes holders. The distance between camera and  $\mu$ PADs can be adjusted. To lower the refraction of the lamp radiations from the inside body of the cabinet, the entire inside of the box is covered with black paint. For capturing images, the  $\mu$ PADs are fixed on a black plastic plate placed in a specified distance to camera. The camera image acquisition parameters are set to auto adjust: ECO mode is on, white balance (keeps colors accurate in deferent lighting) is set on auto, focus range is normal and ISO speed for scene is auto. This designed imaging system can produce highly reproducible images (Hemmateenejad et al. 2010) such that simple subtraction of sample images from blank (or background) image can efficiently correct the light interferences.

## Results and discussion

### Design and fabrication of the $\mu$ PAD

There are different methods for fabrication of  $\mu$ PADs (Li et al. 2010; Xia et al. 2016; Songjaroen et al. 2011). For acidity-base titration, because of higher resistance of wax to acid and base solutions, Karita and Takashi (Karita and Kaneta 2014) used a wax printing method. Since we do not have a wax printing machine, wax dipping as a simple and low-cost fabrication method, which does not require any special tools, was used.

In the designed star-like  $\mu$ PAD devices, the reaction zones are in analogy to the different titration steps and the pH of the buffer in the zones reads the pH of different titration steps. Thus, the pH of each reaction zone plays an important role in the determination of acidity constant. In this regard, keeping a constant pH condition in reaction zones is a challenge. Here, Britton–Robinson buffer as a universal pH buffer was used in the pH range from 2.0 to 12.0. Another important issue is the effect of paper on the pH of buffer solution. Some papers with acidic character in their pH might be between 6 and 7. For balancing the

pH of paper and removing other contaminations from the surface of paper, the papers were firstly (before patterning) washed with doubly distilled water by putting one end in water and allowing the water to diffuse in it by capillary action. Nevertheless, the low acidity of paper has a diminished effect on the pH of buffer solutions. To ensure that the paper does not change the pH of buffer, a piece of the washed paper was formed in a backer-like shape and it was filled with the buffer solution and let to stand for 10 min. Then, the pH of buffer was measured by a pH meter. For all used buffer solutions, no significant differences were found between the measured pH of buffers in glass backers and in paper backers (i.e., the difference were within the range of experimental error).

In our approach, 30.0  $\mu\text{l}$  portion of indicator solution was utilized for the whole hydrophilic zone in the  $\mu\text{PAD}$ . According to the method described by Dungchai and co-workers (2010) and Karita and Kaneta (2014), the volume of the indicator required to fill each reaction zone was calculated. To do so, various volumes of a colored solution were exerted to the  $\mu\text{PADs}$  to fill the entire hydrophilic zone. The areas were measured using AutoCAD software. Volume of the reaction zone was obtained by multiplying required volume to stow the entire channel by the area ratio of each zone in the whole channel (see Table S1, ESI<sup>†</sup>). The volume required to occupy each reaction zone was computed

as 1.2  $\mu\text{l}$ . Considering 0.3  $\mu\text{l}$  volume of the buffer spotted in the reaction zone, moving indicators to the reaction zones causes 4 times dilution of the buffer, which originally was about 0.04 M. In a separate experiment in glassware, it was found that 4-times dilution of buffer did not affect the pH significantly. Thus, it can be assumed that the pH in reaction zones does not change by indicator solution.

To gain higher accuracy, the assay of pKa was achieved by using two  $\mu\text{PADs}$  for each indicator. In the first  $\mu\text{PAD}$ , the pH range of color change was determined for each indicator. In this regard, the pH of the zones is changed from acidic to basic in unit pH interval such that the 9 zones of the  $\mu\text{PAD}$  span about 8 pH units. Once the range of pH with suitable color change is obtained, a second  $\mu\text{PAD}$  with narrow pH range of its zones is used. In the right side of Figs. 2 and 3 are shown the response of the designed  $\mu\text{PADs}$  for the 4 studied indicators including bromocresol green (BG), bromocresol purple (BP), bromothymol blue (BB) and phenolphthalein (PP).

An important issue that should be considered in the imaging-based methods is the type of devices used to record the images. Digital scanners and digital cameras have been widely used and compared (e.g., see Martinez et al. 2008). Scanners work under light control conditions, but the images of two opposite edges of the sample are recorded at different times. On the other hand, digital cameras can record the

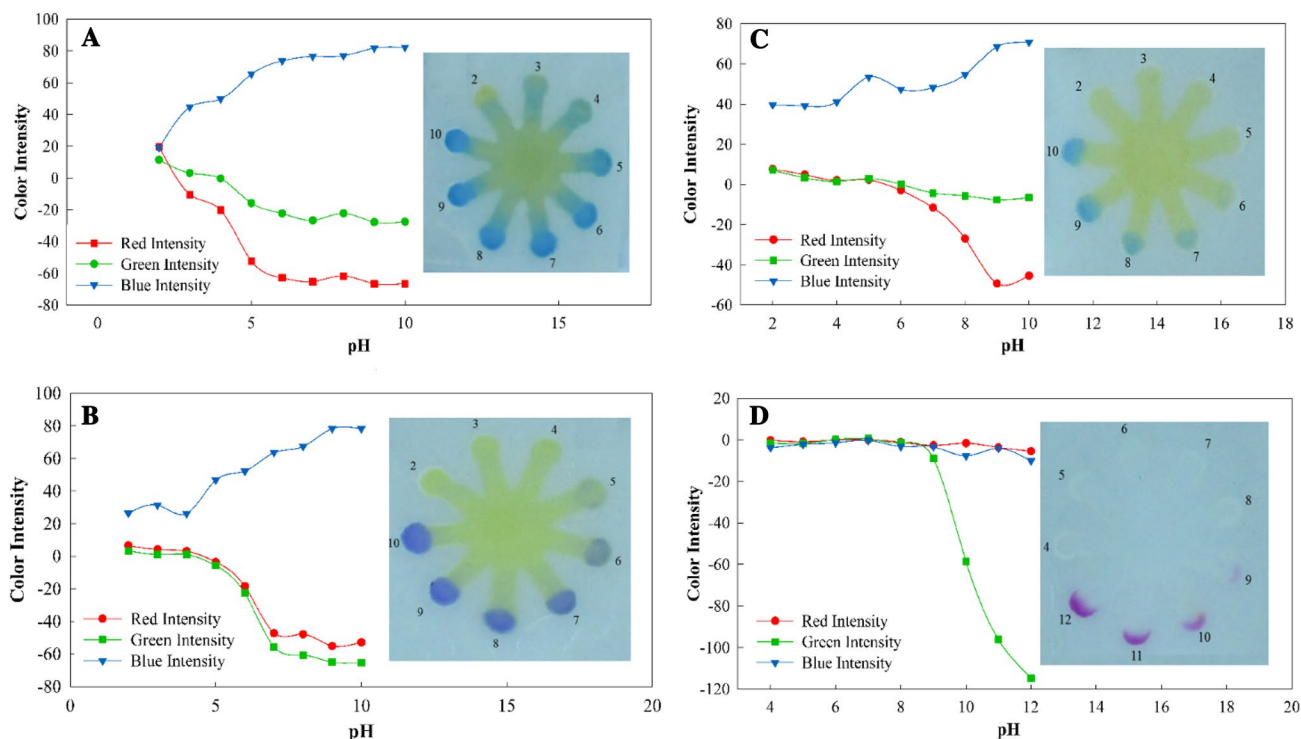


**Fig. 2** Response of the fabricated  $\mu\text{PAD}$  to four studied indicators in a wide pH range of 2–10 in pH intervals of 1.0: **a** BG, **b** BP, **c** BB and **d** PP. Inside: images of  $\mu\text{PADs}$  after loading various indicator solutions

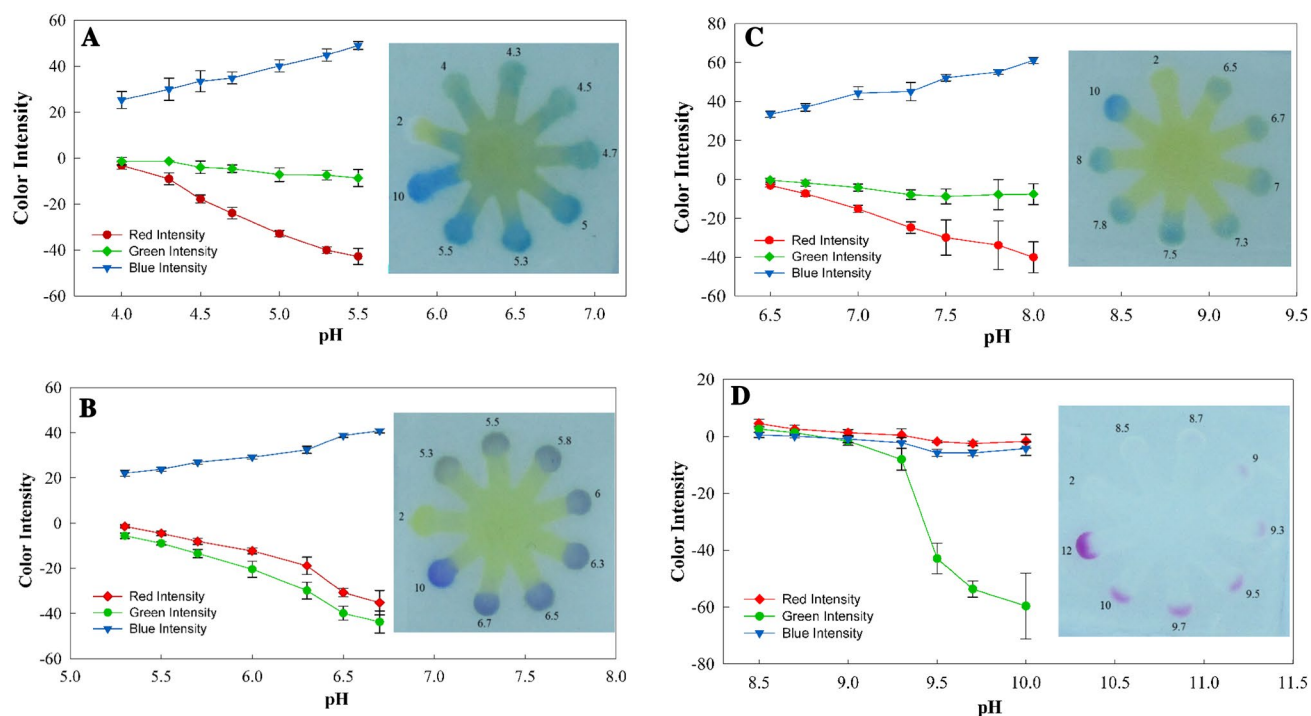


**Fig. 3** Response of the fabricated  $\mu$ PAD to four studied indicators in a narrow pH range and pH intervals of 0.3: **a** BG, **b** BP, **c** BB and **d** PP. The error bars are the standard deviation of three replicate measurements. Inside: images of  $\mu$ PADs after loading various indicator solutions

whole image in very short time, but environmental lights can affect the recorded images. Martinez et al. stated that digital cameras can produce images as high quality as scanners in the controlled lighting conditions. As it was explained in the “Experimental” section, we previously developed a homemade light-controlled digital camera-based imaging system (Hemmateenejad et al. 2014, 2012, 2010) that provides high-quality images with high signal-to-noise ratio and we used it in this study.

### Effect of time on the response of the $\mu$ PAD

Another important parameter that should be considered is the time of reading images after sample injection. The capillary flow of indicator solutions in the paper can be described by Washburn equation;  $L^2 = \gamma Dt/4\eta$ , where  $L$  is the travel distance,  $\gamma$  is the surface tension,  $D$  is the effective pore diameter,  $t$  is the travel time and  $\eta$  is the viscosity (Li et al. 2014). Assuming similar surface tension and effective pore diameter and travel distance for all indicators, the travel time can only depend on the viscosity. The viscosity of the indicators’ solutions was measured using an Ostwald viscometer and was calculated relative to the viscosity of the water as 1.14, 1.09, 1.12, 1.26 for BG, BP, BB and PP, respectively. Since the solutions have very similar viscosity, a similar travel time is assumed for all studied indicators.

After loading of indicator solutions on the central zone, it took 30 s to reach to the reaction zone. This means that color changes were observed in reaction zone 30 s after sample loading. To investigate the effect of color change process, the change in the RGB color intensity of reaction zone was monitored over time. As it is observed in Fig. 1 for the indicators BG, BB and BP, the responses are almost stable for 100 s. However, for PP, as was expected, the color is not stable and fades immediately after reaching the reaction zone. To have higher sensitivity and to achieve as high as possible reproducibility for this indicator, the measured color intensity 30 s after sample loading was used as analytical signal. For other BP indicators, we could use times between 30 and 100 s; however, to have similar conditions for all indicators, the response time of 30 s was also considered for BG, BB and BP.

The schematic procedure for inexpensive determination dissociation constant in pH indicators using  $\mu$ PAD is shown in Fig. S3, ESI†.

Obviously, in the case of first three indicators, by changing pH from acid to basic values the yellow color changed to blue whereas for PP a change of colorless to pink is observed. The changes in the color values of the zones as function of pH are given in Figs. 2 and 3.

## Color intensity calculation and acidity constant determination

The mean color intensities of each reaction zone (in red, green and blue color elements) were calculated with software designed in MATLAB (Mathworks Inc.). In the subroutine written for processing and analyzing of the images, the captured images of  $\mu$ PAD, saved in JPG format was imported in MATLAB, using the ‘‘imread’’ function. (Hemmateenejad et al. 2010). The software allows the user to perform the following operations:

1. To select all or a user-defined particular area of an image.
2. To select inside the selected area in previous step a reference pixel with obvious color change (by mouse clicking) and to calculate R, G and B values of this pixel.
3. To determine all pixels inside the selected area with R, G and B value similar to those of reference values with a tolerance level (degree of similarity) set by the user.
4. To calculate the average of R, G and B value of all assigned pixels in step 3.
5. To export data in a spreadsheet format such that can be loaded in Microsoft Excel.

Since the average color intensity in the reaction zone is calculated, the heterogeneity of the coloring does not affect repeatability. Elimination of background effect and ambient light interferences on RGB also the blank signal was necessary for calculating of analytical signal. For this purpose, first of all, average of intensity color for R, G and B was calculated for each reaction zone ( $A_{1R}$ ) and sample zone ( $A_{1S}$ ), separately, and then they were subtracted from each other ( $A_1$ ) according to Eq. (1). This procedure was also done for the blank  $\mu$ PAD ( $A_B$ ) according to Eq. (2). The final signal was obtained by subtraction of  $A_B$  from  $A_1$  ( $A$ ) according to Eq. (3):

$$A_1 = A_{1R} - A_{1S}, \quad (1)$$

$$A_B = A_{BR} - A_{BS}, \quad (2)$$

$$A = A_1 - A_B. \quad (3)$$

As seen, the resulting color intensity–pH curves show a more or less sigmoidal behavior, similar to the pH–titration curves. For indicators BG, BP and BB, there is an increase in the blue element by increasing pH, while a reverse relationship is observed for the red and green elements. However, in the case of PP, the red and blue elements remain almost constant over the studied pH, whereas by increasing pH a sharp decrease in green element is observed. From these curves, it is possible to have a raw estimate of acidity constant.

To have a more accurate estimation, further data analysis is required. The dissociation reaction of an indicator in aqueous solution can be schematically represented with the simple Eq. (4):



where HIn and  $\text{In}^-$  represent the acidic and basic forms of pH indicator, respectively. Then, the known Henderson–Hasselbalch Eq. (5) can be found from the equilibrium constant of this reaction. For determination of pKa values, this helpful equation can be written in the following way (Klotz et al. 2011):

$$\text{pH} = \text{pKa} + \log \frac{\text{In}^-}{\text{HIn}}, \quad (5)$$

where pKa is the apparent acidity constant (Dávila et al. 2013).

In this case, a plot of  $\log(\text{In}^-/\text{HIn})$  against pH would produce a straight line with an intercept of pKa. For each reservoir zone of  $\mu$ PAD, the data of the curves shown in Fig. 4 were used to calculate the ratio of  $\text{In}^-/\text{HIn}$  as:

$$\frac{\text{In}^-}{\text{HIn}} = \frac{(A - A_{\text{In}^-})}{(A_{\text{HIn}} - A)}, \quad (6)$$

where  $A_{\text{HIn}}$  and  $A_{\text{In}^-}$  are the color intensity of the indicator in its acidic (HIn) and basic forms, respectively, and  $A$  is color intensity at each pH (or each zone). The values of  $A_{\text{HIn}}$  and  $A_{\text{In}^-}$  can be taken from two extreme pH values in Fig. 3. Also, in the second  $\mu$ PAD (Fig. 3), two zones were filled with buffer solutions of the lowest and highest pH values (used for determination of  $A_{\text{HIn}}$  and  $A_{\text{In}^-}$ , respectively) and the remaining 7 zones were filled with buffers, at which color changes were observed. The RGB color values were used for determination of  $A$ ,  $A_{\text{HIn}}$  and  $A_{\text{In}^-}$ . For each indicator, individual color elements of R, G and B and their binary (R + G, R + B and B + G) or ternary (R + B + G) combinations were used separately to plot Eq. (5) and the one resulted in the best regression line (based on lower fitting error) was selected for calculation of pKa. Based on this assumption, the individual color elements of R, G, B and G were used for the indicators BG, BP, BB and PP, respectively.

Figure 4 displays a graphical representation of Eq. (5) for the four studied indicators. The intercept and slope values of Eq. (5) were then computed through a linear regression analysis. Interestingly, for all indicators, the obtained plots showed a linear relationship with good correlation coefficients, except PP, for which the correlation coefficient is not so good. As it was explained previously (effect of time on the response of the  $\mu$ PAD), the color of PP fades fast and there is an uncertainty in the recording the color change of PP when it reaches to the detection zone. Nevertheless,

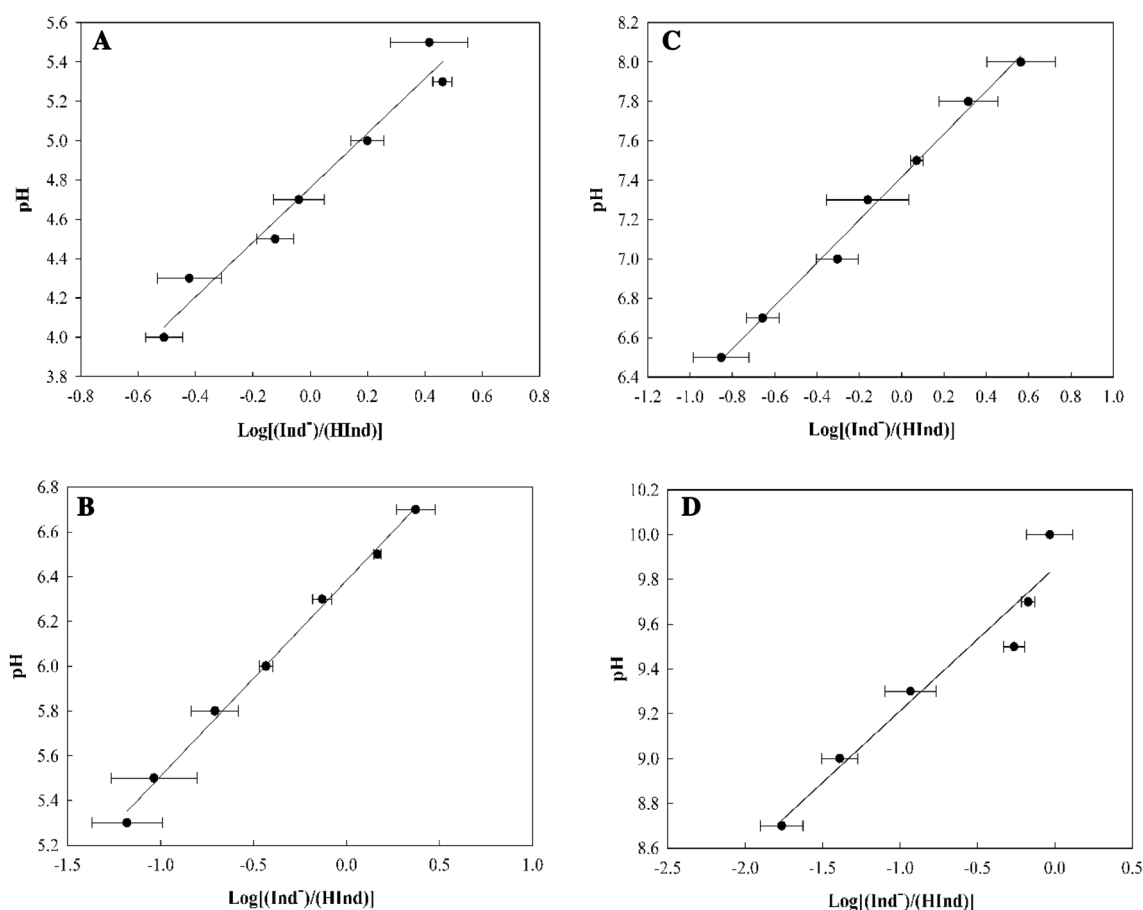


**Fig. 4** Henderson–Hasselbalch plots based on the curves obtained in Figs. 2 and 3. **a** BG, **b** BP, **c** BB and **d** PP

**Table 1** Characteristics of the Henderson–Hasselbalch regression equations obtained for different indicators and the corresponding calculated acidity constants

pH indicators	Slope	Intercept	$R^2$	pKa calculated	RSD % ( $n = 3$ )	pKa (Patnaik 2004; Dean 1992) reported
Bromocresol green	1.4294	4.7636	0.9888	4.76	2.18	4.7
Bromocresol purple	1.1333	6.3219	0.9867	6.32	0.55	6.3
Bromothymol blue	1.0905	7.4170	0.9927	7.42	1.25	7.1
Phenolphthalein	0.6392	9.8518	0.9390	9.85	0.73	9.4

as observed from Table 1, the estimated pKa of PP by this method is very close to the literature value.

Thus, the intercept can be taken as an estimate of the pKa values of the indicators. As is obvious from Table 1, the estimated pKa values by  $\mu$ PAD devices are very close to the corresponding literature values (obtained by the spectrophotometric method). One example of the pKa calculation on  $\mu$ PAD is demonstrated in the ESI for make it more clarification (S5, ESI<sup>†</sup>).

In the Henderson–Hasselbalch equation, the concentrations should be represented by ( $\text{In}^-$ ) and ( $\text{HIn}$ ). The Henderson–Hasselbalch equation can be also used in the

case of polyprotic acids, as long as the consecutive pKa values differ by at least 2 (better 3). It should be noted that the species of phenolphthalein, bromocresol purple, bromocresol green and bromothymol blue are considered to be divalent. It is difficult to discriminate pKa<sub>1</sub> and pKa<sub>2</sub> for them. Thus in the protocol presented here, only one pKa was determined, as reported previously.

In addition to high accuracy in pKa determination by  $\mu$ PAD devices, they also offered reproducible results. The relative standard deviations in reported pKa values for three reproduced experiments was found to be less than 5%.

## Conclusions

We developed a simple and fast acidity constant determination method based on  $\mu$ PAD technology that needs no appliance and sophisticated instrumentation like spectrophotometer (Fig S4). This  $\mu$ PAD consists of reaction zones, which are detection zones too. They contain constant amounts of the buffer with different pH. The titration is completed within 1 min, including the time required for sample application. By recording the image of reaction zones of different pH and plotting color intensities over pH (according to Henderson–Hasselbalch equation), the acidity constant of indicators can be easily calculated. It was used to determine acidity constants of 4 indicators and close agreement with the literature values were obtained. This  $\mu$ PAD is more advantageous than classic titrimetry in terms of speed, portability, disposability, small volume of reagents and sample and does not necessitate sophisticated appliances and instrumentation like spectrophotometer, it is affordable and cost-effective at a much lower cost although the number of significant figures is less. Therefore, when compared to the conventional method that uses large amounts of reagent, takes more time, and is an expensive spectrophotometer and titrator, we can save much money, time, and the operator fee. A set of 50  $\mu$ PADs could be made in under 2 h and at a materials cost of under \$0.07 per PAD. The cost per PAD, with labor at \$10 per hour, is about \$0.47.

In summary, we introduced a simple and rapid method for colorimetric determination of the acid dissociation constant of indicators by employing  $\mu$ PAD analytical devices fabricated via the wax dipping method. Without a need for any glassware or professional equipment, the pKa can be determined directly by a very low volume of solutions. Compared to the spectrophotometric methods, the invented method in this work offers much lower cost and higher speed and is more environmentally friendly. We would like to emphasize that the  $\mu$ PAD can be used to determine the acid dissociation constant of only colorful reagents and it is limited to those that undergo color change by dissociation.

**Acknowledgements** This work was supported by the Shiraz University Research Council.

## References

- Čadková E, Komárek M, Debord J, Puppa LD, Bordas F, Bollinger JC (2013) PKa Constant determination of two triazole pesticides: tebuconazole and penconazole. *J Solut Chem* 42(5):1075–1082. <https://doi.org/10.1007/s10953-013-0012-z>
- Dávila YA, Sancho MI, Almandoz C, Blanco SE (2013) Solvent effects on the dissociation constants of hydroxy flavones in organic-water mixtures. determination of the thermodynamic P K a values by UV-visible spectroscopy and DFT calculations. *J Chem Eng Data* 58:1706–1716
- Dean JA (1992) Lange's handbook of chemistry. Fifteenth. McGraw-Hill, New York
- Demiralay EÇ, Duygu Koç Y, Daldal D, Cakır C (2012) Determination of chromatographic and spectrophotometric dissociation constants of some beta lactam antibiotics. *J Pharm Biomed Anal* 71(December):139–143. <https://doi.org/10.1016/j.jpba.2012.06.023>
- Dungchai W, Chailapakul O, Henry CS (2010) Use of multiple colorimetric indicators for paper-based microfluidic devices. *Anal Chim Acta* 674(2):227–233. <https://doi.org/10.1016/j.aca.2010.06.019> (Elsevier BV)
- Gao B, Liu H, Zhongze G (2014) Bottom-up fabrication of paper-based microchips by blade coating of cellulose microfibers on a patterned surface. *Langmuir* 30(50):15041–15046. <https://doi.org/10.1021/la503720b>
- Gluck SJ, Steele KP, Benkö MH (1996) Determination of acidity constants of monoprotic and diprotic acids by capillary electrophoresis. *J Chromatogr A* 745(1):117–125. [https://doi.org/10.1016/0021-9673\(96\)00386-X](https://doi.org/10.1016/0021-9673(96)00386-X)
- Hemmateenejad B, Mobaraki N, Shakerizadeh-Shirazi F, Miri R (2010) Multivariate image analysis-thin layer chromatography (MIA-TLC) for simultaneous determination of co-eluting components. *The Anal* 135(7):1747. <https://doi.org/10.1039/c0an00078g>
- Hemmateenejad B, Akhond M, Mohammadpour Z, Mobaraki N (2012) Quantitative monitoring of the progress of organic reactions using multivariate image analysis-thin layer chromatography (MIA-TLC) method. *Anal Methods* 4(4):933. <https://doi.org/10.1039/c2ay25023c>
- Hemmateenejad B, Farzam SF, Mobaraki N (2014) Simultaneous measurement of leucine and isoleucine by multivariate image analysis-thin layer chromatography (MIA-TLC). *J Iran Chem Soc* 11(6):1609–1617. <https://doi.org/10.1007/s13738-014-0433-7>
- Jayawardane BM, Wei S, McKelvie ID, Kolev SD (2014) Microfluidic paper-based analytical device for the determination of nitrite and nitrate. *Anal Chem* 86(15):7274–7279. <https://doi.org/10.1021/ac5013249>
- Jokerst JC, Adkins JA, Bisha B, Mentele MM, Goodridge LD, Henry CS (2012) Development of a paper-based analytical device for colorimetric detection of select foodborne pathogens. *Anal Chem* 84(6):2900–2907. <https://doi.org/10.1021/ac203466y>
- Karita S, Kaneta T (2014) Acid–base titrations using microfluidic paper-based analytical devices. *Anal Chem* 86(24):12108–12114. <https://doi.org/10.1021/ac5039384>
- Klotz E, Doyle R, Gross E, Mattson B (2011) The equilibrium constant for bromothymol blue: a general chemistry laboratory experiment using spectroscopy. *J Chem Educ* 88(5):637–639. <https://doi.org/10.1021/ed1007102>
- Li X, Tian J, Shen W (2010) Progress in patterned paper sizing for fabrication of paper-based microfluidic sensors. *Cellulose* 17:649–659. <https://doi.org/10.1007/s10570-010-9401-2>
- Li H, Han D, Pauletti GM, Steckl AJ (2014) Blood coagulation screening using a paper-based microfluidic lateral flow device. *Lab Chip* 14(20):4035–4041. <https://doi.org/10.1039/C4LC00716F>
- Martinez AW, Phillips ST, Butte MJ, Whitesides GM (2007) Patterned paper as a platform for inexpensive, low-volume, portable. *Angew Chem Int Ed* 46(8):1318–1320. <https://doi.org/10.1002/anie.200603817>
- Martinez AW, Phillips ST, Carrilho E, Thomas SW, Sindi H, Whitesides GM (2008) simple telemedicine for developing regions: camera phones and paper-based microfluidic devices for real-time, off-Site diagnosis. *Anal Chem* 80(10):3699–3707. <https://doi.org/10.1021/ac800112r>
- Mentele MM, Cunningham J, Koehler K, Volckens J, Henry CS (2012) Microfluidic paper-based analytical device for particulate metals. *Anal Chem* 84(10):4474–4480. <https://doi.org/10.1021/ac300309c>
- Nan G, Shi J, Huang Y, Sun J, Lv J, Yang G, Li Y (2014) Dissociation constants and solubilities of daidzein and genistein in



- different solvents. *J Chem Eng Data* 59(4):1304–1311. <https://doi.org/10.1021/jc4010905>
- Nie Z, Nijhuis CA, Gong J, Chen X, Kumachev A, Martinez AW, Narovlyansky M, Whitesides GM (2010) Electrochemical sensing in paper-based microfluidic devices. *Lab Chip* 10(4):477–483. <https://doi.org/10.1039/B917150A>
- Oosterbroek E, Van den Berg A (2003) *Lab-on-a-chip: miniaturized systems for (bio)chemical analysis and synthesis*, 2nd edn. Elsevier, Amsterdam
- Patnaik P (2004) *Dean's analytical chemistry handbook*, 2nd edn. McGraw-Hill, New York
- Rattanarat P, Dungchai W, Cate D, Volckens J, Chailapakul O, Henry CS (2014) Multilayer paper-based device for colorimetric and electrochemical quantification of metals. *Anal Chem* 86(7):3555–3562. <https://doi.org/10.1021/ac5000224>
- Schilling KM, Lepore AL, Kurian JA, Martinez AW (2012) Fully enclosed microfluidic paper-based analytical devices. *Anal Chem* 84(3):1579–1585. <https://doi.org/10.1021/ac202837s>
- Songjaroen T, Dungchai W, Chailapakul O, Laiwattanapaisal W (2011) Novel, simple and low-cost alternative method for fabrication of paper-based microfluidics by wax dipping. *Talanta* 85(5):2587–2593. <https://doi.org/10.1016/j.talanta.2011.08.024> (Elsevier BV)
- Songjaroen T, Dungchai W, Chailapakul O, Henry CS, Laiwattanapaisal W (2012) Blood separation on microfluidic paper-based analytical devices. *Lab Chip* 12(18):3392–3398. <https://doi.org/10.1039/c2lc21299d>
- Wang S, Ge L, Song X, Yu J, Ge S, Huang J, Zeng F (2012) Paper-based chemiluminescence ELISA: lab-on-paper based on chitosan modified paper device and wax-screen-printing. *Biosens Bioelectron* 31(1):212–218. <https://doi.org/10.1016/j.bios.2011.10.019> (Elsevier BV)
- Wang P, Ge L, Ge S, Jinghua Y, Yan M, Huang J (2013) A paper-based photoelectrochemical immunoassay for low-cost and multiplexed point-of-care testing. *Chem Commun* 49(32):3294–3296. <https://doi.org/10.1039/c3cc00149k>
- Xia Y, Si J, Li Z (2016) Fabrication techniques for microfluidic paper-based analytical devices and their applications for biological testing: a review. *Biosens Bioelectron* 77:774–789. <https://doi.org/10.1016/j.bios.2015.10.032> (Elsevier BV)
- Xu Y, Phillips JA, Yan J, Qingge Li Z, Fan H, Tan W, Box PO (2009) Aptamer-based microfluidic device for enrichment, sorting, and detection of multiple cancer cells. *Anal Chem* 81(17):7436–7442
- Yu J, Ge L, Huang J, Wang S, Ge S (2011a) Microfluidic paper-based chemiluminescence biosensor for simultaneous determination of glucose and uric acid. *Lab Chip* 11(7):1286. <https://doi.org/10.1039/c0lc00524j>
- Yu J, Wang S, Ge L, Ge S (2011b) A novel chemiluminescence paper microfluidic biosensor based on enzymatic reaction for uric acid determination. *Biosens Bioelectron* 26(7):3284–3289. <https://doi.org/10.1016/j.bios.2010.12.044> (Elsevier BV)